

Closed shell effects from the stability and instability of deformed and superdeformed nuclei against cluster decays in the mass regions 130-158 and 180-198

Raj K. Gupta, Sharda Dhaulta, Rajesh Kumar and M. Balasubramaniam
Physics Department, Panjab University, Chandigarh-160014, India.

G. Münzenberg
Gesellschaft für Schwerionenforschung mbH, Planckstrasse 1, D-64291 Darmstadt, Germany.

Werner Scheid
Institut für Theoretische Physik, Justus-Liebig-Universität, Heinrich-Buff-Ring 16, D-35392 Giessen, Germany.
(November 2, 2018)

The stability and/or instability of the deformed and superdeformed nuclei, ${}_{60}^{133-137}\text{Nd}$, ${}_{64}^{144-158}\text{Gd}$, ${}_{80}^{176-194}\text{Hg}$, and ${}_{82}^{192-198}\text{Pb}$ parents, coming from three regions of different superdeformations, are studied with respect to the α and heavy cluster decays. The α -decay studies also include the heavier ${}^{199-210}\text{Pb}$ nuclei, for reasons of spherical magic shells at $Z=82$ and $N=126$. The calculations are made by using the preformed cluster-decay model, and the obtained α -decay half-lives are compared with the available experimental data. Having met with a very good success for the comparisons of α -decay half-lives and in giving the associated known magic or sub-magic closed shell structures of both the parent nuclei and daughter products, the interplay of closed shell effects in the cluster-decay calculations is investigated. The cluster-decay calculations also give the closed shell effects of known spherical magicities, both for the parent and daughter nuclei, and further predict new (deformed) closed shells at $Z=72-74$ and $N=96-104$ due to both the stability and instability of Hg and Pb parents against cluster decays. Specifically, a new deformed daughter radioactivity is predicted for various cluster decays of ${}^{186-190}\text{Hg}$ and ${}^{194,195}\text{Pb}$ parents with the best possible measurable cases identified as the ${}^8\text{Be}$ and ${}^{12}\text{C}$ decays of ${}^{176,177}\text{Hg}$ and/or ${}^{192}\text{Pb}$ parents. The predicted decay half-lives are within the measurable limits of the present experimental methods. The interesting point to note is that the parents with measurable cluster decay rates are normal deformed nuclei at the transition between normal and superdeformation.

I. INTRODUCTION

The α -decay results have been used for identifying the shell closure effects for quite some time now, including even the very weak, sub-shell closures. For example, the $Z=64$ sub-shell was first noted by observing the systematics of α -decay energies [1], and later by a dip at $Z=64$ in the measured α -decay reduced widths [2], of a few $N=84$ isotones in its neighborhood. In the recent past, some of us and collaborators [3–9] have coupled the α -decay studies with the exotic cluster-decay result of the observed spherical closed-shell daughter (${}^{208}\text{Pb}$ or a neighbouring nucleus), called cluster radioactivity [10–12]. This allowed us to predict two other new spherical closed-shell

daughter radioactivities, namely ${}^{100}\text{Sn}$ and ${}^{132}\text{Sn}$ daughter radioactivities [4–7], and also a deformed daughter radioactivity at $Z=74-76$ and $N=98-104$ [8]. The spherical ${}^{100}\text{Sn}$ daughter radioactivity has been emphasized also by Poenaru, Greiner and Gherghescu [13], and a couple of, so-far unsuccessful, experimental attempts have also been made to observe it as the ground-state decay of ${}^{114}\text{Ba}$ nucleus produced in heavy-ion reactions [14,15]. This decay is now believed to belong to an excited compound nucleus decay, studied for ${}^{12}\text{C}$ decay of ${}^{116}\text{Ba}^*$ [16,17]. Furthermore, the cluster decay studies are also used to point out the shell stabilizing effects of the parent nucleus [3,8,9]. Thus, both the cases of large and small decay rates (equivalently, the small and large decay half-lives) are found important, the large ones referring to closed shell effects of the daughter nucleus and the small ones to closed shell effects of the parent nucleus. In other words, taking a clue from the experiments, in a decay calculation, the presence of a known spherical or deformed daughter should result in a large decay rate (small decay half-life) or alternatively, a large decay rate (small decay half-life) should refer to the existence of a known or un-known (new), spherical or deformed, closed shell for the daughter nucleus.

In the above mentioned calculations, we have so-far investigated the alpha and/or cluster decays of various neutron-deficient and neutron-rich rare-earths ${}_{54}\text{Xe}$ to ${}_{64}\text{Gd}$ [4–7] and the even- A deformed and superdeformed ${}_{80}^{180-194}\text{Hg}$ nuclei [8]. In mercury nuclei, the superdeformation begins at the ${}^{189}\text{Hg}$ isotope, and the axes ratios are $\approx 1.7:1$ [18]. Note that the superdeformation here refers to the observation of (excited) superdeformed band(s) in these nuclei, though their ground-state deformations are not very much different from other neighbouring nuclei. This is illustrated in Fig. 1, where the data for ground-state quadrupole deformation parameter β_2 is taken from the calculations of Möller et al. [19], since a similar data from experiments is not available for all the nuclei studied here. On the other hand, a deformed or normal deformed nucleus is one where superdeformed band(s) are not observed and it comes from the well known mass region $150 < A < 190$ of deformation. In the above stated nuclei, the closed shell effects of

both the daughter products and the parent nuclei were analyzed. The stability of parent nuclei was also studied for the mass region $A=68-82$ [3,9], which includes several deformed and superdeformed nuclei (here, both in the ground states). However, there are several other regions of various deformations and superdeformations in the mass regions $A=130-158$ and $180-198$ [18] whose decay characteristics still remain to be probed. The aim of this paper is to make a complete analysis of the decay properties of nuclei in these two mass regions, in order to get a general picture of how the deformed, in particular the superdeformed, nuclei behave against the α and heavier cluster decays. The superdeformed nuclei are expected to be more instable, though, like for the mass region $A=68-82$ [3,9], the following analysis does not seem to support this contention. Instead, the superdeformed nuclei are found to be rather poor α emitters, as compared to their lower mass, normal deformed nuclei. They are, however, shown to be the better α emitters than the heavier mass (heavier than superdeformed nuclei), normal deformed nuclei. The same is found true for cluster decay results. Such an un-expected situation is presented by the presence of known and/or un-known (new) closed shell effects of the daughter products. Also, the closed shell effects of either the protons or neutrons, as well as the neutron/proton asymmetry, of the parent nucleus play a role.

The other nuclei that have superdeformations identical to those of $^{189-194}_{80}\text{Hg}$ nuclei are the $^{191}_{79}\text{Au}$, $^{191-195}_{81}\text{Tl}$, $^{192-196,198}_{82}\text{Pb}$ and $^{197}_{83}\text{Bi}$ nuclei. Then, there are several rare-earths, from ^{62}Sm to ^{66}Dy and ^{68}Er , which have even more strongly superdeformed shapes with axes ratios $\approx 2:1$. Also, some other rare-earths, the ^{57}La to ^{60}Nd , have superdeformed species with axes ratios $\approx 1.5:1$. In this paper, we choose to work specifically with both the odd- and even- A $^{133-137}_{60}\text{Nd}$, $^{144-158}_{64}\text{Gd}$ and $^{182-198}_{82}\text{Pb}$ parents, which comprise the three regions of different superdeformations mentioned above, along with some normal deformed nuclei. Note that $^{154-158}\text{Gd}$ are known α -stable nuclei, but are found to be of interest from the point of view of heavy-cluster instabilities and the associated closed shell effects (Section III.B.2). We have also included in our analysis here, the already studied [8] mercury nuclei, extended to both the odd- and even- A $^{176-194}_{80}\text{Hg}$, and the heavier $^{199-210}\text{Pb}$ nuclei where some experimental data for α -decays are available. Thus, the cases of both the normal deformed and superdeformed nuclei, and the spherical closed shell nuclei at and around $Z=82$, $N=126$, are covered in our study. Figure 1 shows that all the superdeformed nuclei chosen here come from the transition (both lighter and heavier) regions of known deformed nuclei in the mass region $150 < A < 190$.

The paper is organised as follows. The calculations are made by using the preformed cluster-decay model (PCM) of Gupta and collaborators [20–23] whose brief outline is presented in section II. Section III deals with the calculations and results obtained from this study. A

summary of our results and conclusions are presented in section IV.

II. THE PREFORMED CLUSTER-DECAY MODEL

The preformed cluster-decay model (PCM) is a well established method for cluster decay studies. We refer the reader to original papers [20–22] or the reviews in Refs. [12,23] for complete details on the model. In the PCM, the decay constant λ (or, inversely, the decay half-life time $T_{1/2}$) is the product of the cluster preformation probability P_0 , the barrier impinging frequency ν_0 , and the barrier penetration probability P ,

$$\lambda = \frac{\ln 2}{T_{1/2}} = P_0 \nu_0 P. \quad (1)$$

For calculating P_0 and P , the authors introduced, respectively, the dynamical collective coordinate of mass asymmetry $\eta=(A_1-A_2)/A$, with $A=A_1+A_2$, and relative separation R between the two fragments, via the stationary Schrödinger equation

$$H(\eta, R)\psi_n(\eta, R) = E_n\psi_n(\eta, R). \quad (2)$$

The potential part of the Hamiltonian in this equation is defined by

$$V(\eta, R) = \sum_{i=1}^2 B_i(A_i, Z_i) + \frac{Z_1 Z_2 e^2}{R} + V_p, \quad (3)$$

given as the sum of the experimental binding energies [24] and the Coulomb and nuclear proximity [25] potentials. The fragmentation potential $V(\eta)$ and the scattering potential $V(R)$ are obtained from Eq. (3), respectively, for fixed R and η . The R is fixed at the touching configuration, $R=C_t=C_1+C_2$, the C_i being the Süssmann central radii $C_i = R_i - 1/R_i$ (in fm) with R_i as the equivalent spherical radii $R_i = 1.28A_i^{1/3} - 0.76 + 0.8A_i^{-1/3}$ fm; and η is fixed by the emitted cluster. The charges Z_i in (3) are fixed by minimizing the potential (without V_p) in the charge asymmetry coordinate $\eta_Z=(Z_1-Z_2)/Z$, with $Z=Z_1+Z_2$.

In principle, the two coordinates are coupled, but in view of the defining equation (1), the Schrödinger equation (2) is solved in the decoupled approximation of η and R -motions. Only the ground-state ($n=0$) solution is relevant for the cluster decay to occur in the ground-state of the daughter nucleus. Then, for η motion, the properly normalized fractional cluster preformation probability is

$$P_0(A_2) = |\psi(\eta)|^2 \sqrt{B_{\eta\eta}(\eta)} \frac{2}{A}, \quad (4)$$

with $B_{\eta\eta}$ taken as the classical hydrodynamical mass of Kröger and Scheid [26]. For the R -motion, we use the

WKB approximation for calculating the penetrability P . In PCM, the penetration is considered to begin at $R = R_a = C_t$ and end at $V(R_b) = Q$ -value of the decay.

Finally, the impinging frequency ν_0 in the PCM is defined by considering that the total kinetic energy, shared between the two fragments, is the positive Q -value. Then,

$$\nu_0 = \frac{\text{velocity}}{R_0} = \frac{\sqrt{2Q/mA_2}}{R_0}. \quad (5)$$

Here R_0 is the equivalent spherical radius of the parent nucleus and mA_2 is the mass of emitted cluster.

III. CALCULATIONS

In this section, we present our calculations first for α -decay, compared with the experimental data, wherever available. Then, we analyze the cluster-decay calculations with a view to look for the role of known magic shells in both the daughter and parent nuclei, and the possible new closed-shell daughter products presenting the signatures of a new radioactivity, if any. The cluster decay calculations are presented separately for each set of nuclei.

Figures 2 and 3 show the fragmentation potentials for Nd and Pb nuclei, as the representatives of the two mass regions ($A=130-158$ and $180-198$) studied here. The experimental binding energies used are from the 1995 tables of Audi and Wapstra [24]. We notice that in each case, the potential energy minima occur at ${}^4\text{He}$ and other $N=Z$, α nuclei, as well as at $N \neq Z$, non- α nuclei for all the parents in the heavier mass region ($A=180-198$) and for only the heavier parents in the lighter mass region $A=130-158$. This means that the α -nuclei decay products are energetically more favoured for the lighter isotopes of Nd and Gd parents in the lighter mass region $A=130-158$, and the non- α decay products become equally favourable for all the Hg and Pb parents in the heavier mass region $A=180-198$ and for the heavier isotopes of Nd and Gd parents in $A=130-158$ mass region. We are interested only in the potential energy minima because the preformation factors P_0 for nuclei at the minima are the largest, compared to their neighbours, as is depicted in Fig. 4 for Nd and Gd and in Fig. 5 for Hg and Pb parents, where, for some clusters belonging to the minima in the fragmentation potentials, the (negative) logarithm of the preformation probability P_0 is plotted as a function of the mass number of the parents. We notice that in all cases, like in our earlier calculations [3–9], the preformation factor is largest for ${}^4\text{He}$ and it goes on decreasing as the size of the cluster increases. Another point of interest to note in these figures is the change of clusters for the heavier parents (see the dashed parts of lines). For example, in both the Figs. 4 and 5, the cluster ${}^{16}\text{O}$ for ${}^{144-154}\text{Gd}$ and ${}^{176-193}\text{Hg}$ nuclei changes to ${}^{16}\text{C}$ for heavier ${}^{155-158}\text{Gd}$ and ${}^{194}\text{Hg}$ nuclei. However,

then the Q -value (for ${}^{16}\text{C}$ cluster combination) is so small (see Fig. 6) that the penetrability is almost negligible (and hence of not much interest to include such clusters any further in our analysis). Figure 6 also reveals that the Q -value is negative (or nearly zero) for α -decay of ${}^{146}\text{Gd}$, and for both the α and ${}^8\text{Be}$ decays of Gd nuclei heavier than ${}^{154}\text{Gd}$. The fact that the penetrabilities P are small ($-\log_{10}P$ large) for smaller Q -values, is evident from Figs. 7 and 8, which give, similar to Figs. 4 and 5, the results of our calculation for the barrier penetrability P . We further notice in Fig. 7 that the penetrability P is in general small (large $-\log_{10}P$) for non- α clusters in the light mass region $A=130-158$. The combined effect of the preformation probability P_0 and penetrability P gives the measurable decay half-life time $T_{1/2}$, since the impinging frequency ν_0 is almost constant. The resulting $T_{1/2}$ are presented in Figs. 9 and 10, where their logarithms are plotted with respect to the mass number of the parent nuclei. The structural information obtained from these calculations for each set of parents is discussed separately in the following sub-sections. Note, however, in Fig. 9(b) that ${}^{154}\text{Gd}$ is almost stable against α and ${}^8\text{Be}$ decays (large $T_{1/2}$ -values), but could be of interest for other heavier cluster decays, as is discussed in section III.B.2.

A. The α -decay results

We have noted above that the preformation factor P_0 is largest for ${}^4\text{He}$. This is of the order of $10^{-5} - 10^{-8}$ for all superdeformed ${}^{133-137}\text{Nd}$, superdeformed and some heavier mass, normal deformed ${}^{144-154}\text{Gd}$ nuclei (superdeformation in Gd nuclei stops at ${}^{150}\text{Gd}$, and Gd nuclei beyond ${}^{154}\text{Gd}$ are α -stable, $Q_\alpha < 0$; Q -value is small but positive for α -decay of ${}^{154}\text{Gd}$, though experimentally it is a known α -stable nucleus), all superdeformed and some lighter mass (mainly odd- A), normal deformed ${}^{183-194}\text{Hg}$ (here superdeformation begins at ${}^{189}\text{Hg}$) and all superdeformed ${}^{192-198}\text{Pb}$ nuclei. However, P_0 is much larger, $\sim 10^{-3}$, for almost all lighter mass, normal deformed ${}^{176-188}\text{Hg}$ and ${}^{182-191}\text{Pb}$ nuclei. This suggests that superdeformed nuclei are the poorer α -emitters, as compared to their light mass, normal deformed species. Interesting enough, the same result is born out in the calculated α -decay half-lives $T_{1/2}^\alpha$, plotted in Fig. 11 as $\log_{10}T_{1/2}^\alpha$ versus parent mass number, and compared with the available experimental data (taken from Refs. [27,28]). We have also included here (see inset, Fig. 11) the other heavier isotopes of Pb in order to include the lone experimental data for ${}^{210}\text{Pb}$, in the neighborhood of doubly magic ${}^{208}\text{Pb}$ nucleus. The Fig. 11 presents not only the interesting comparison of calculated results with experiments, but also interesting shell structure effects of both the parent nuclei and their daughter products which are mostly known but not yet observed experimentally via α -decay studies (the α -decay experimental data are

not yet complete). We have also compared our results and the available experimental data with another calculation due to the generalized liquid drop model (GLDM) [27] in Table 1. We notice that the PCM and the GLDM calculations give identical results, both within one order of magnitude of the experimental data.

The following results are evident from Fig. 11: (i) The PCM calculations compare nicely with experiments, showing even the (small) odd-even effects in both the light mass, normal deformed $^{176-188}\text{Hg}$ and $^{182-191}\text{Pb}$ nuclei. The odd-even effects seem to become weaker in all the superdeformed and heavier normal deformed nuclei studied here (see e.g. $^{148-152}\text{Gd}$ or $^{189-194}\text{Hg}$ nuclei). The data are not yet enough to show the odd-even effects as clearly as are given by the calculations. The comparison between the experimental data and our calculations for all the five $^{148-152}\text{Gd}$ isotopes (containing no apparent odd-even effects) and the single ^{210}Pb parent in very heavy mass region are also particularly striking. (ii) The light mass, normal deformed $^{176-188}\text{Hg}$ and $^{182-191}\text{Pb}$ parents are clearly the better α emitters (smaller $T_{1/2}^\alpha$ values), as compared to their heavier and superdeformed counterparts and the superdeformed $^{133-137}\text{Nd}$ and $^{144-154}\text{Gd}$ parents. This also includes the heavier, normal deformed $^{151-154}\text{Gd}$ nuclei. However, the superdeformed nuclei are better α emitters than the heavier mass, normal deformed nuclei. In other words, the superdeformed nuclei are though better α emitters than the heavier mass, normal deformed (heavier than the superdeformed) nuclei, but both are poorer α emitters as compared to the light mass, normal deformed nuclei. (iii) The large (peaking of) $T_{1/2}^\alpha$ -values for ^{146}Gd and $^{207,208}\text{Pb}$ parents show the shell closure effects (strong stability) of magic $N=82$ and 126 coupled with their semi-magic $Z=64$ and magic $Z=82$, respectively. (iv) The above noted peaking effect of $T_{1/2}^\alpha$ at the spherical magic shells of the parents could be interpreted as the signature of the change of a shell from the deformed to the spherical one or one can say the presence of a (spherical or deformed) closed-shell daughter at the bottom(s) or valley(s) of such a peak. One such result is evident for the minimum (valley) at ^{148}Gd , which refers clearly to $N=82$ spherical daughter $^{144}_{62}\text{Sm}$ for its α decay. A similar minimum at ^{134}Nd could be due to the mid-shell effect of magic $Z=50$ and sub-magic $Z=64$ for the (weakly deformed) daughter $^{130}_{58}\text{Ce}$. Such peaking effects are also visible in the superdeformed Hg and Pb nuclei. Apparently, all these results clearly establish the credentials of PCM for its possible predictions for the heavier-cluster decays and the associated shell structure effects, studied in the following sub-section.

B. The heavy cluster-decays and closed-shell effects

We have seen above, and is also known from our earlier calculations [4-7,9], that as the $N:Z$ ratio of parent

nuclei increases, the $N \neq Z$, non- α nuclei cluster emissions become equally, or even more, probable as compared to $N=Z$, α nuclei cluster emissions (see, e.g., the crossing over of the curves for ^{12}C and ^{14}C clusters in Fig. 4(b) for heavier Gd parents or in Fig. 5(a) for Hg parents; P_0 becomes larger for ^{14}C , as compared to that for ^{12}C). Hence, the α -nucleus cluster emission effects must be more prevalent for parents in the low mass region $A=130-158$ and the non- α nuclei cluster emissions for parents in the heavier mass region $A=180-198$. We know that all the radioactive exotic cluster-decays from the parent masses $A > 222$ consist of only non- α nuclei clusters [12], such as ^{14}C , $^{18,20}\text{O}$, ^{23}F , $^{22,24,26}\text{Ne}$, $^{28,30}\text{Mg}$ and $^{32,34}\text{Si}$. Secondly, it is interesting to note that, though the cluster preformation factors P_0 are of similar orders for both the chosen regions of parent nuclei (compare Figs. 4 and 5), the penetrabilities P are much smaller (larger $-\log_{10}P$) for parents in the lighter mass region $A=130-158$ (compare Figs. 7 and 8). This means that, like for α -decays, the cluster-decay rates for parents in the lighter mass region are also expected to be smaller (larger cluster-decay half-lives) than for parents in the heavier mass region. In other words, the parents in lighter mass region $A=130-158$ are likely to be more stable against cluster decays, than the parents in heavier mass region $A=180-198$. We discuss these results in the following for each set of parent nuclei separately.

1. Nd parents

First of all we look at the calculations in Figs. 4(a) and 7(a), respectively, for the preformation probability P_0 and penetrability P for Nd parents. We notice that $-\log_{10}P_0$ for the lightest two clusters ^8Be and ^{12}C are structure-less (remains almost constant), but for heavier clusters develop into maxima (minima for P_0) each at the even- A parents ^{134}Nd and ^{136}Nd which grow as the size of the cluster increases. On the other hand, for the penetrability, $-\log_{10}P$ is structure-less for all clusters, except for a steep rise for ^8Be decay and small maximum (minimum for P) at ^{134}Nd (or a minimum at ^{135}Nd) for its ^{14}C decay. The fact that these maxima and minima are simply the result of an odd-even effect in Nd nuclei is evident from the almost constant cluster decay half-lives $T_{1/2}^c$ in Fig. 9(a). The notable exception is again for ^8Be decay, where the decay half-life is an ever increasing function of parent mass, with $T_{1/2}^c > 10^{100}(\text{s})$ and hence stable against such a decay. The interesting result is that some heavy clusters, like $^{30,32}\text{Si}$, have decay half-lives of the same order as for the light clusters like ^{12}C and ^{16}O . These are apparently due to, say, the neighbouring $Z=50$ magic shell in $^{119}_{52}\text{Te}$ daughter, or the mid-shell effects of the known neutron magic shells, in ^{16}O decay of ^{135}Nd parent. The decay half-lives are, however, large $\sim 10^{50}$ (s). In other words, the Nd parents are as stable, rather more stable, against cluster decays as they are against

α -decays.

2. Gd parents

For Gd parents, the P_0 in Fig. 4(b) seem to behave smoothly, except for a small minimum at ^{148}Gd parent, which turn into a minimum at ^{145}Gd and a maximum at ^{148}Gd parent for the heavier clusters. Also, the division between the superdeformed and normal deformed nuclei is evident at ^{152}Gd where P_0 increases suddenly ($-\log_{10}P_0$ decreases) for all the clusters and stays nearly independent of the mass of normal deformed parents (except for small oscillations, the odd-even effect). On the other hand, the P in Fig. 7(b) show the maxima, minima structure for different light clusters at any one of the parent nuclei $^{146-152}\text{Gd}$. The heavier clusters are all peaked around ^{146}Gd . These results combine to give four significant minima for $T_{1/2}^c$ in Fig. 9(b): one at ^{150}Gd for ^8Be decay, another at ^{152}Gd for ^{12}C decay, the third one at ^{154}Gd for ^{14}C decay and finally the fourth one at ^{156}Gd for ^{18}O decay. All these minima refer to $N=82$ magicity of the respective daughters $^{142}_{60}\text{Nd}$, $^{140}_{58}\text{Ce}$, $^{140}_{58}\text{Ce}$ and $^{138}_{56}\text{Ba}$. In other words, these are the only four isotopes of Gd ($^{152-156}\text{Gd}$) which are prone to heavier cluster decays, though the predicted decay half-lives are large $\sim 10^{43-10^{67}}$ (s). Note that one of these parents (^{150}Gd) is a superdeformed nucleus whereas the other three heavier ones ($^{152,154,156}\text{Gd}$) are normal deformed nuclei. Also, of these four, ^8Be and ^{12}C decays of ^{150}Gd and ^{152}Gd , respectively, are more probable (smaller $T_{1/2}^c$). Then, there are some maxima appearing in Fig. 9(b), mainly at ^{146}Gd , which refer to the stability of this parent nucleus against the cluster decays due to its $N=82$ shell closure. Note that ^{146}Gd is already stable against ^8Be decay ($Q < 0$). Thus, the structure effects of both the parent(s) and daughters come into play in the cluster-decay properties of Gd nuclei, but the predicted cluster decay half-lives are beyond the limits of the present measurements, which go only upto $\sim 10^{28}$ (s) [12].

3. Hg parents

In this sub-section, we discuss the results of our calculations for normal deformed $^{176-188}\text{Hg}$ and superdeformed $^{189-194}\text{Hg}$ nuclei, presented in Figs. 5(a), 8(a) and 10(a) for P_0 , P and $T_{1/2}^c$, respectively. First of all, we notice a number of minima and maxima in Fig. 5(a) for P_0 , which correspond to the odd-even effects of the parents. Then, the P_0 increases suddenly ($-\log_{10}P_0$ decreases) near the transition point of deformed to superdeformed region where it has the largest value for almost all the cluster preformations in ^{188}Hg , the normal deformed nucleus at the transition. As we shall see below for the $T_{1/2}^c$ calculations, this result corresponds exactly to the one observed for the α -decay half-lives of Gd isotopes in

Fig. 11, i.e. of the change of shape in going from a maximum (peaking) to the minimum (valley). On the other hand, the P are nearly smooth functions of the parent mass, except for a noticeable minimum (enhanced penetrability) at ^{185}Hg , and/or for some clusters at ^{189}Hg , in Fig. 8(a). The resulting $T_{1/2}^c$ in Fig. 10(a) show interesting maxima and minima, like for P_0 , for normal deformed $^{176-185}\text{Hg}$ nuclei, referring to the larger stability of the even parents (at maxima) relative to the odd parents (at minima). Then, a (broad) minimum or valley of instability (smaller values next to a maximum in $T_{1/2}^c$) occurs for the normal deformed and superdeformed transitional nuclei $^{186-190}\text{Hg}$.

The above noted stability of even-A $^{176-185}\text{Hg}$ nuclei point to the closed shell effects of these parents at $Z=80$ (in the neighborhood of magic $Z=82$) coupled with a magic or semi-magic nature of their neutron shells with $N=96,98,100,102$ and 104 . On the other hand, the instability of $^{186-190}\text{Hg}$ parents, against various clusters, reflect the closed shell effects of the daughter nuclei, like $^{178-182}\text{Os}$, $^{174-178}\text{W}$, .., etc., referring to $Z=76,74,..$ and $N=106,104,102,..$ closed or near-closed shells. Coupling the results of both the stability and instability in this region, with the fact that ^8Be and ^{12}C are shown as the most probable cluster decays (smallest $T_{1/2}^c$ -values), the $Z=76$ or 74 and $N=96-104$ seem to point to the major (deformed) closed shells. The same result was obtained in our earlier studies [4,8] and supports the structure calculations of other authors [29,30]. Also, Fig. 10(a) shows that the best measurable ^8Be and ^{12}C decays come from $^{176,177}\text{Hg}$, with $T_{1/2}^{8\text{Be}} \sim 10^{18}$ (s) and $T_{1/2}^{12\text{C}} \sim 10^{23}$ (s), which are well within the limits of present day experiments.

4. Pb parents

The calculations for Pb parents are presented in Figs. 5(b), 8(b) and 10(b), respectively, for P_0 , P and $T_{1/2}^c$. The P_0 are almost constant, except for a small enhancement (minimum $-\log_{10}P_0$) in the case of ^{196}Pb parent for all cluster configurations. The same is true for the P , except that the enhancement is now for the ^{195}Pb parent. The net result is a shallow minimum in $T_{1/2}^c$ for heavier clusters, like ^{20}O and ^{24}Ne , from ^{194}Pb or ^{195}Pb parents, which means the shell stabilizing effects of the daughters $^{174,175}_{74}\text{W}$ and $^{170,171}_{72}\text{Hf}$. This means supplementing the above noted results for Hg isotopes that the major closed shells could even occur at $Z=72,74$, $N=98-100$. The minimum decay half-lives are for the ^8Be and ^{12}C decays of ^{192}Pb , both $\sim 10^{37}$, which are still not within the reach of experiments.

IV. SUMMARY OF RESULTS AND CONCLUSION

We have made a systematic study of the α - and heavy-cluster decays of nuclei with masses $A=130-158$ and $180-198$, comprising three regions of superdeformations to different orders. Specifically, the $^{133-137}\text{Nd}$, $^{144-158}\text{Gd}$, $^{176-194}\text{Hg}$ and $^{192-198}\text{Pb}$ nuclei are studied, which also include the normal deformed nuclei on both the lighter and heavier sides of the superdeformed nuclei. Furthermore, for α -decay of Pb nuclei, we have also considered the very heavy isotopes upto ^{210}Pb which means including also the spherical closed shell effects of ^{208}Pb with doubly magic $Z=82$ and $N=126$. The main idea of this work is to look for new (spherical or deformed) closed shells via cluster decay studies or, in other words, the possible signatures of any new cluster radioactivity in the superdeformed nuclei. A parent nucleus is stable against α and other cluster-decays, if the decay half-lives are large. On the other hand if the decay half-life is small (measurable or close to measurable) then, in view of the so-far observed radioactive decays, it must refer to the closed shell effects of the daughter product(s). Based on such an analysis for both the α and heavier cluster decays, we have obtained the following results from the chosen nuclear mass regions.

The superdeformed nuclei are better α emitters, as compared to their heavier mass, normal deformed isotopes, though both of these are poorer α emitters than their lighter mass, normal deformed species. The closed shell effects of the parents (for ^{146}Gd and ^{208}Pb parents), at the spherical sub-magic $Z=64$, magic $N=82$ and doubly magic $Z=82$, $N=126$, are evident in terms of the maxima or peaking of the α -decay half-lives, whereas the same for daughter nuclei ^{130}Ce and ^{144}Sm (for ^{134}Nd and ^{148}Gd parents, respectively) are given as minima or valleys in α -decay half-lives due to the mid-shell effect of the magic $Z=50$ and sub-magic $Z=64$, and the $N=82$ magic shell. These are the known shell closure effects, which apparently are nicely reproduced in the PCM calculations.

The calculated cluster-decay half-lives show that the lighter mass region $A=130-158$ is more stable (larger $T_{1/2}^c$ values) than the heavier mass region $A=180-198$. The light mass region presents the closed shell effects of known magic $Z=50$ or $N=82$ shells (for ^{16}O decay of ^{135}Nd , ^8Be decay of ^{150}Gd , $^{12,14}\text{C}$ decays of $^{152,154}\text{Gd}$, respectively, and ^{18}O decay of ^{156}Gd), with the predicted cluster decay half-lives beyond the present measurable limits of the experiments ($T_{1/2}^c \sim 10^{43}$ (s) or more). On the other hand, the heavier mass region $A=180-198$ present not only the stability effects of neighbouring $Z=82$ magic shell for even- A $^{176-185}\text{Hg}$ parents, but also interesting new possibilities of deformed-daughter cluster radioactivity at $Z=72-76$ and $N=96-104$ for $^{186-190}\text{Hg}$ and $^{194,195}\text{Pb}$. In other words, new deformed magic shells are likely to occur at $Z=72-76$ and $N=96-104$ for various cluster decays of $^{186-190}\text{Hg}$ and $^{194,195}\text{Pb}$. The best,

observable cases are predicted to be ^8Be and ^{12}C decays of $^{176,177}\text{Hg}$ and/or ^{192}Pb parents (with $T_{1/2}^c \sim 10^{18}$ and 10^{23} (s), respectively). The interesting point is that in both the nuclear regions under study, more of these nuclei are normal deformed nuclei rather than superdeformed ones. In fact, they lie at the transition between the normal deformation and superdeformation, but more towards the region of normal deformation. The best possible cases also come from the normal deformed regions. In other words, the region of the change of shape, i.e. the valley(s) in the immediate neighbourhood of a peak, seems to be the criterion for the location of new magicities or for the new cluster radioactivity(ies).

V. ACKNOWLEDGMENTS

This work is supported in parts by the Council of Scientific and Industrial Research (CSIR), India, and the VW-Stiftung, Germany.

-
- [1] J.O. Rasmussen, S.G. Thompson, and A. Ghiorso, Phys. Rev. **89**, 33 (1953).
 - [2] W.-D. Schmidt-Ott and K.S. Toth, Phys. Rev. C **13**, 2574 (1976).
 - [3] R.K. Gupta, W. Scheid, and W. Greiner, J. Phys. G: Nucl. Part. Phys. **17**, 1731 (1991).
 - [4] R.K. Gupta, S. Singh, R.K. Puri, and W. Scheid, Phys. Rev. C **47**, 561 (1993).
 - [5] S. Kumar and R.K. Gupta, Phys. Rev. C **49**, 1922 (1994).
 - [6] S. Kumar, D. Bir, and R.K. Gupta, Phys. Rev. C **51**, 1762 (1995).
 - [7] S. Kumar, J.S. Batra, and R.K. Gupta, J. Phys. G: Nucl. Part. Phys. **22**, 215 (1996).
 - [8] R.K. Gupta, D. Bir, and S. Dhaulta, Mod. Phys. Lett. A **12**, 1775 (1997).
 - [9] R.K. Gupta, S. Dhaulta, R. Bonetti, and W. Scheid, J. Phys. G: Nucl. Part. Phys. **25**, 1089 (1999).
 - [10] A. Săndulescu, D.N. Poenaru, and W. Greiner, Sovt. J. Part. Nucl. **11**, 528 (1980).
 - [11] H.J. Rose and G.A. Jones, Nature **307**, 245 (1984).
 - [12] R.K. Gupta and W. Greiner Int. J. Mod. Phys. E **3**, 335 (1994, Suppl.).
 - [13] D.N. Poenaru, W. Greiner, and R. Gherghescu, Phys. Rev. C **47**, 2030 (1993).
 - [14] Yu.Ts. Oganessian, Yu.A. Lazarev, V.L. Mikheev, Yu.A. Muzychka, I.V. Shiokovsky, S.P. Tretyakova, and V.K. Utyonkov, Z. Phys. A **349**, 341 (1994).
 - [15] A. Guglielmetti, B. Blank, R. Bonetti, Z. Janas, H. Keller, R. Kirchner, O. Klepper, A. Piechaczek, A. Plochocki, G. Poli, P.B. Price, E. Roeckel, K. Schmidt, J. Szerypo, and A.J. Westphal, Nucl. Phys. A **583**, 867 (1995).

- [16] M. La Commara, J. Gomez del Campo, A. D'Onofrio, A. Gadea, M. Glogowski, P. Jarillo-Herrero, N. Belcari, R. Borcea, G. de Angelis, C. Fahlander, M. Gorska, H. Grawe, M. Hellström, R. Kirchner, M. Rejmund, V. Roca, E. Roeckl, M. Romano, K. Rykaczewski, K. Schmidt, and F. Terrasi, *Nucl. Phys. A* **669**, 43 (2000).
- [17] R.K. Gupta, M. Balasubramaniam, C. Mazzocchi, M. La Commara, and W. Scheid, *Phys. Rev. C* **65**, 024601 (2002).
- [18] R.B. Firestone and B. Singh, *Table of Superdeformed Nuclear Bands and Fission Isomers*, LBL-35916, UC-413, June 1994.
- [19] P. Möller, J.R. Nix, W.D. Myers and W.J. Swiatecki, *At. Data Nucl. Data Tables*, **59** (1995) 185.
- [20] R.K. Gupta, in *Proc. 5th Int. Conf. on Nuclear Reaction Mechanisms*, Varenna, 1988, edited by E. Gadioli (Ricerca Scientifica ed Educazione Permanente, Milano, 1988), p.416.
- [21] S.S. Malik and R.K. Gupta, *Phys. Rev. C* **39**, 1992 (1989).
- [22] S. Kumar and R.K. Gupta, *Phys. Rev. C* **55**, 218 (1997)
- [23] R.K. Gupta, in *Heavy Elements and Related New Phenomena*, edited by W. Greiner and R.K. Gupta (World Scientific, Singapore, 1999), Vol. **II**, p. 730.
- [24] G. Audi and A.H. Wapstra, *Nucl. Phys. A* **595**, 4 (1995).
- [25] J. Blocki, J. Randrup, W.J. Swiatecki, and C.F. Tsang, *Ann. Phys. (N.Y)* **105**, 427 (1977).
- [26] H. Kröger and W. Scheid, *J. Phys. G* **6**, L85 (1980).
- [27] G. Royer, *J. Phys. G: Nucl. Part. Phys.* **26**, 1149 (2000).
- [28] F. García, O. Rodríguez, M. Goncalves, S.B. Durate, O.A.P. Tavares, and F. Guzmán, *J. Phys. G: Nucl. Part. Phys.* **26**, 755 (2000).
- [29] F. Hannachi, G. Bastin, M.G. Porquet, C. Schüick, J.P. Thibaud, C. Bourgeois, L. Hildingsson, D. Jerrestam, N. Perrin, H. Serrgolle, F.A. Beck, T. Byrski, J.C. Merdinger, and J. Dudek, *Nucl. Phys. A* **481**, 135 (1988).
- [30] D.D. Dracoulis, A.E. Stuchbery, A.O. Macchiavelli, C.W. Beausang, J. Burde, M.A. Deleplanque, R.M. Diamond, and F.S. Stephens, *Phys. Lett. B* **208**, 365 (1988).

Figure Captions:

- Fig. 1. The variation of ground-state quadrupole deformation parameter β_2 with mass number for the selected Nd, Gd, Hg and Pb parent nuclei. The data are from the calculations of Möller et. al [19]. The region of nuclei where superdeformed bands are observed is marked in each case.
- Fig. 2. The mass fragmentation potentials as a function of the mass number of light fragments, for the superdeformed isotopes of Nd parents. The calculations are made at the touching configuration $R=C_1+C_2=C_t$ and by using experimental binding energies [24]. Only the light fragments (clusters) at minima are marked.
- Fig. 3. The same as for Fig. 2, but for both the normal deformed and superdeformed isotopes of Pb parents.
- Fig. 4. The logarithms of the cluster preformation probability P_0 as a function of the mass number of (a) Nd, and (b) Gd parents, for different clusters. For the same cluster mass number, the dashed line shows P_0 if the charge number is changed.
- Fig. 5. The same as for Fig. 4, but for (a) Hg, and (b) Pb parents.
- Fig. 6. The variation of Q-value with mass number for (a) Gd and (b) Hg parents. The binding energies used are the experimental binding energies [24].
- Fig. 7. The same as for Fig. 4, but for the penetrability P .
- Fig. 8. The same as for Fig. 7, but for (a) Hg, and (b) Pb parents.
- Fig. 9. The same as for Fig. 4, but for the logarithms of cluster decay half-life, $\log_{10} T_{1/2}^c(\text{s})$.
- Fig. 10. The same as for Fig. 9, but for (a) Hg, and (b) Pb parents.
- Fig. 11. The logarithm of the calculated α -decay half-lives, $\log_{10} T_{1/2}^\alpha(\text{s})$, as a function of the parent mass number for various isotopes of Nd, Gd, Hg and Pb nuclei, compared with the experimental data (taken from Refs. [27,28]). The inset shows the same calculation for the heavier isotopes of Pb, where the experimental data for only ^{210}Pb is known.

Table 1: The logarithms of α -decay half-lives and other characteristic quantities calculated by using the preformed cluster model (PCM) of Gupta and collaborators. The impinging frequency ν_0 is nearly constant, of the order of $10^{21}s^{-1}$. The PCM calculations are compared with the available GLDM calculations of Royer [27] and the experimental data.

Parent	Q-value (MeV)	PCM		$\log_{10}T_{1/2}(s)$		
		P_0	P	PCM	GLDM	Expt.
¹⁴⁸ Gd	3.27	3.10×10^{-05}	1.38×10^{-28}	10.90	9.68	9.36
¹⁴⁹ Gd	3.10	2.84×10^{-07}	2.84×10^{-29}	13.64	11.15	11.21
¹⁵⁰ Gd	2.81	4.13×10^{-07}	7.13×10^{-31}	15.10	14.09	13.75
¹⁵¹ Gd	2.65	9.41×10^{-08}	5.92×10^{-32}	16.83	15.92	15.11
¹⁵² Gd	2.21	1.02×10^{-05}	2.78×10^{-36}	19.17	22.12	21.54
¹⁷⁶ Hg	6.93	6.21×10^{-03}	9.63×10^{-18}	-2.38	-1.76	-1.7
¹⁷⁷ Hg	6.74	1.36×10^{-04}	4.69×10^{-18}	-0.40	-1.17	-0.77
¹⁷⁸ Hg	6.58	1.82×10^{-03}	2.39×10^{-18}	-1.23	-0.60	-0.44
¹⁷⁹ Hg	6.43	9.57×10^{-05}	1.22×10^{-18}	0.35	-0.04	0.32
¹⁸¹ Hg	6.29	5.36×10^{-05}	6.04×10^{-19}	0.91	0.49	1.32
¹⁸² Hg	6.00	1.29×10^{-03}	1.23×10^{-19}	0.23	1.68	1.85
¹⁸³ Hg	6.04	1.83×10^{-06}	1.62×10^{-19}	2.96	1.50	1.57
¹⁸⁴ Hg	5.66	6.60×10^{-04}	1.49×10^{-20}	1.45	3.20	3.37
¹⁸⁶ Hg	5.21	4.02×10^{-05}	4.49×10^{-22}	4.21	5.40	5.73
¹⁸² Pb	7.08	6.50×10^{-03}	1.57×10^{-17}	-2.61	-1.59	-1.26
¹⁸⁹ Pb	5.86	1.12×10^{-07}	2.57×10^{-20}	4.98	3.17	4.11
¹⁹¹ Pb	5.41	4.64×10^{-07}	8.29×10^{-22}	5.87	5.31	5.78
²¹⁰ Pb	3.79	2.48×10^{-09}	2.63×10^{-30}	16.74	16.00	16.57

Fig. 1 "Closed shell effects from" R.K. Gupta et al.

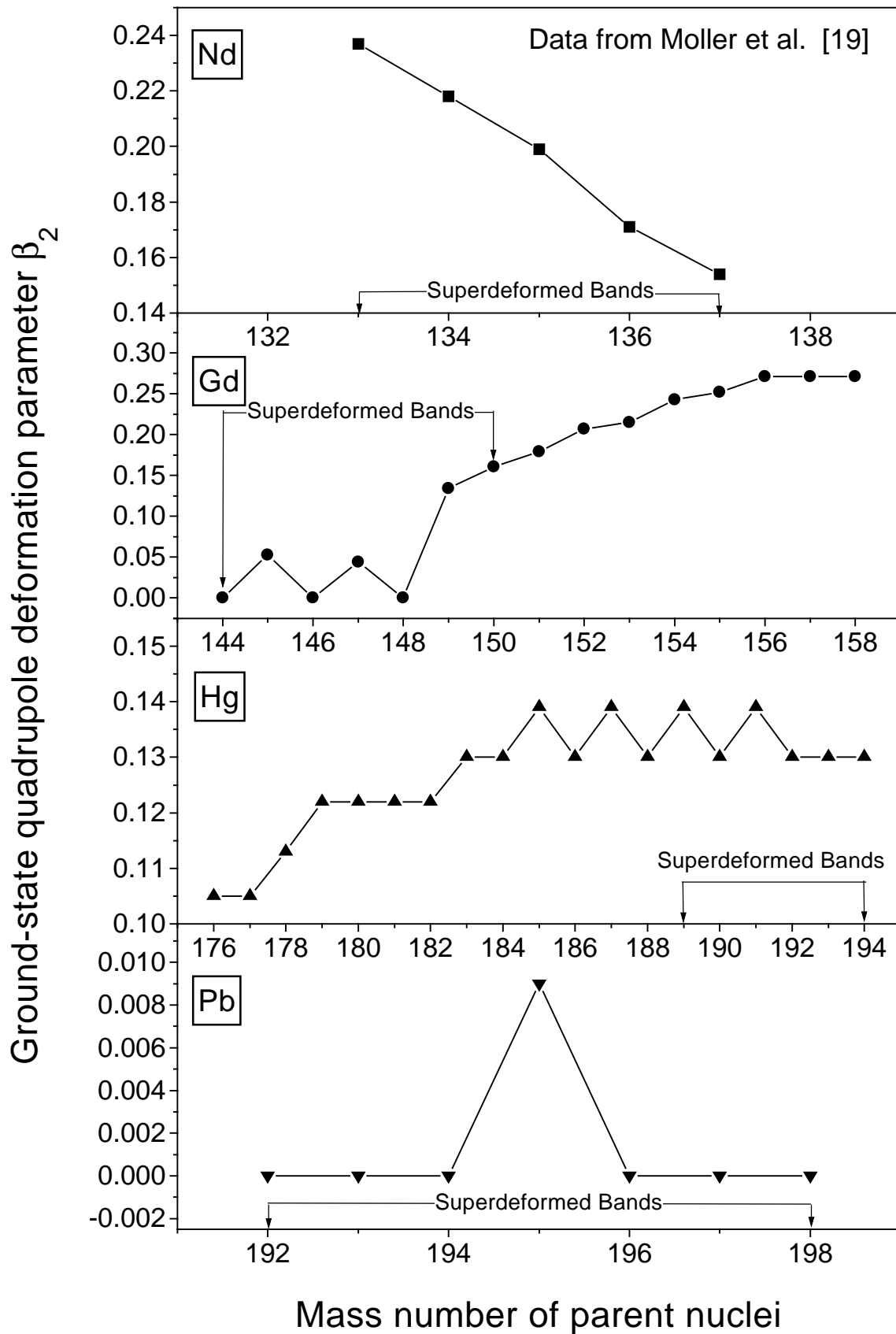


Fig. 2 "Closed shell effects from" R.K. Gupta et al.

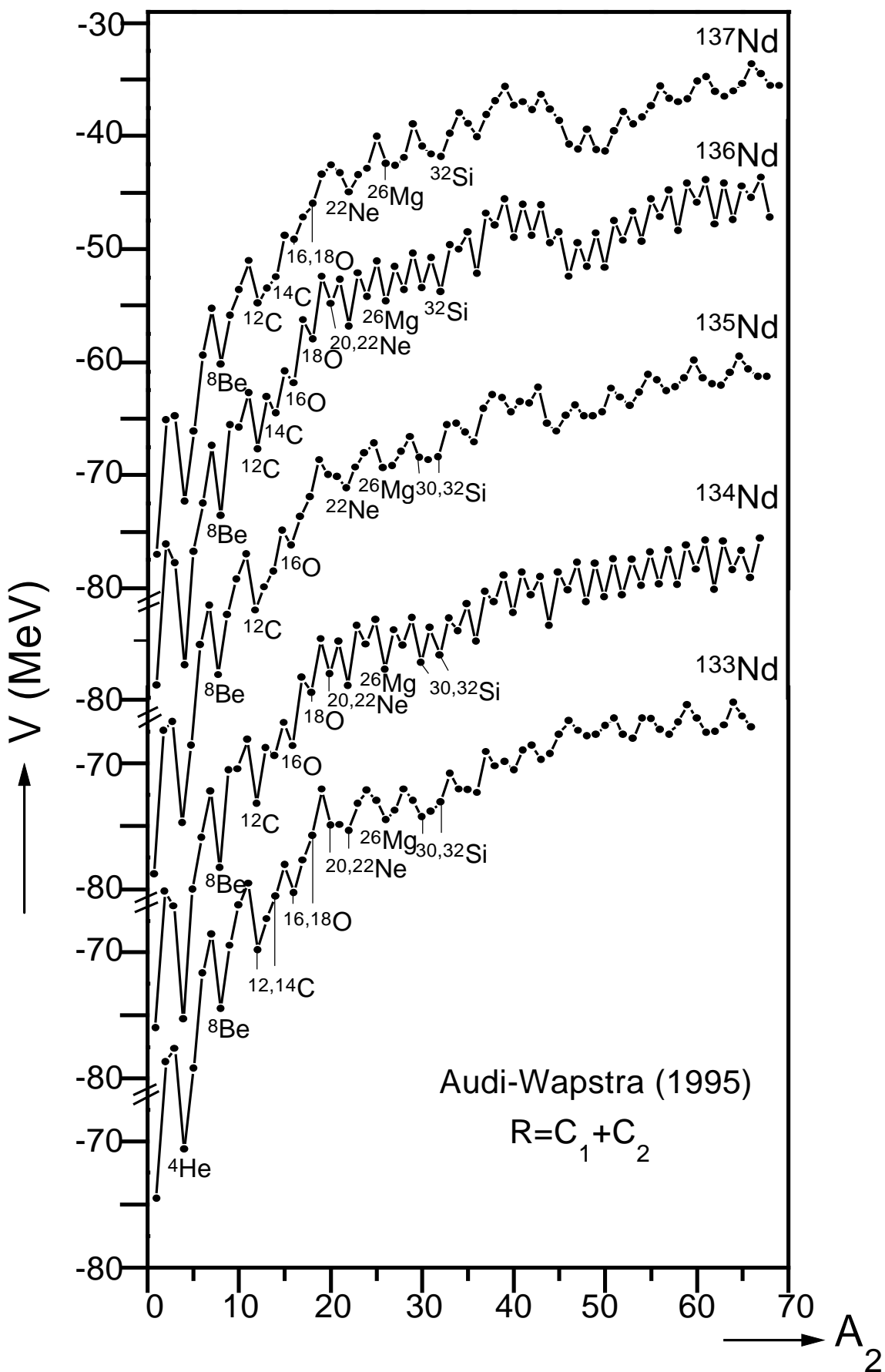


Fig. 3 "Closed shell effects from" R.K. Gupta et al.

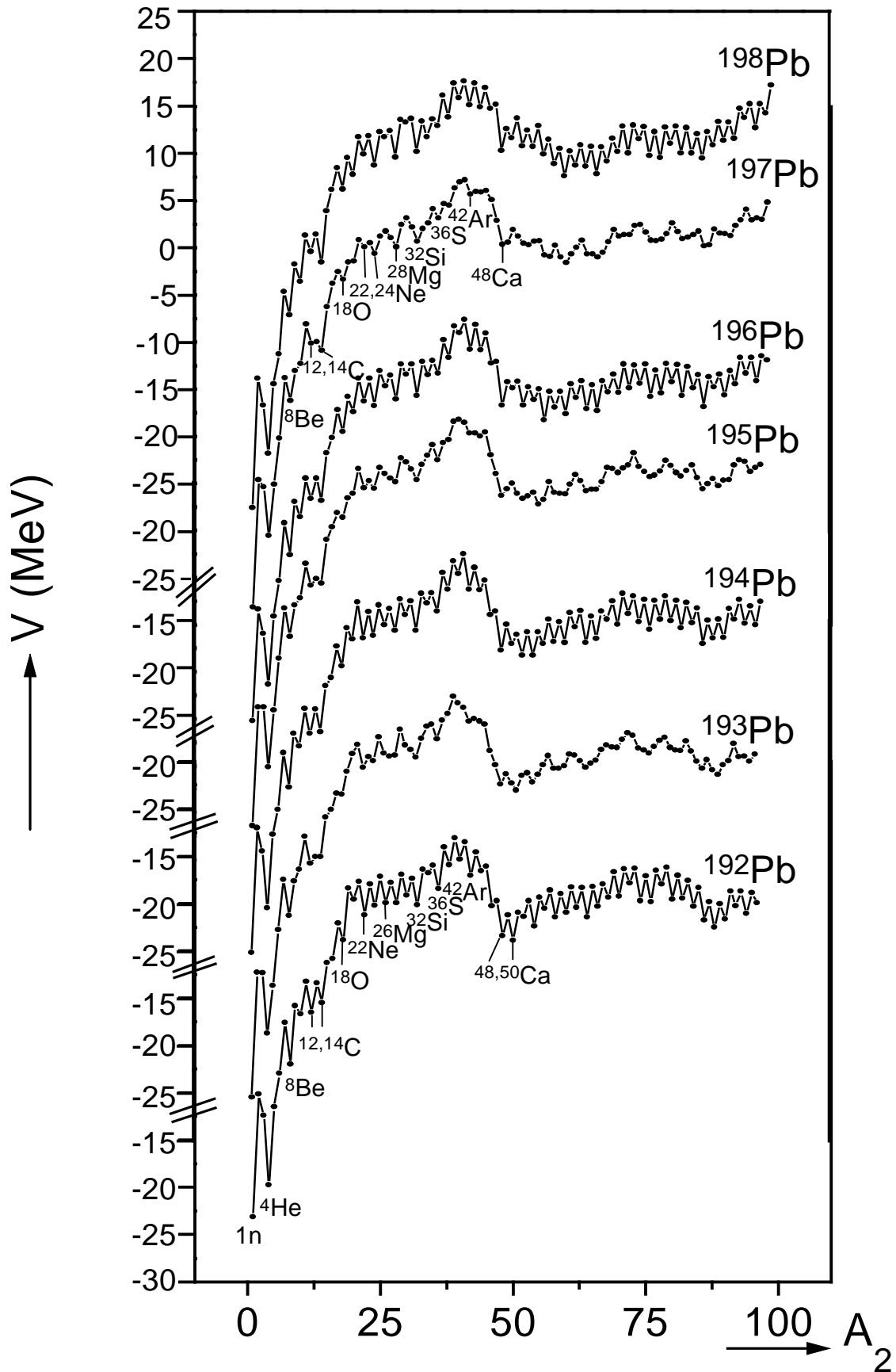


Fig. 5 "Closed shell effects from" R.K. Gupta et al.

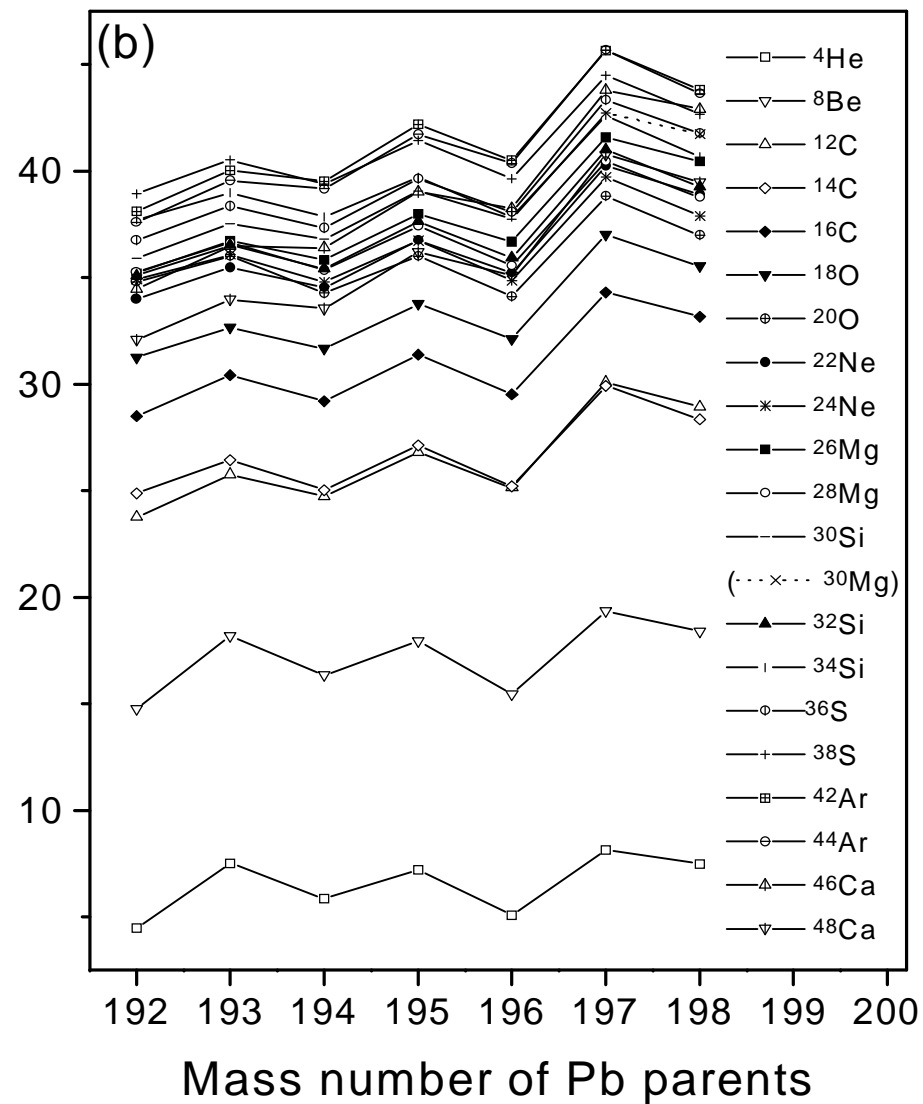
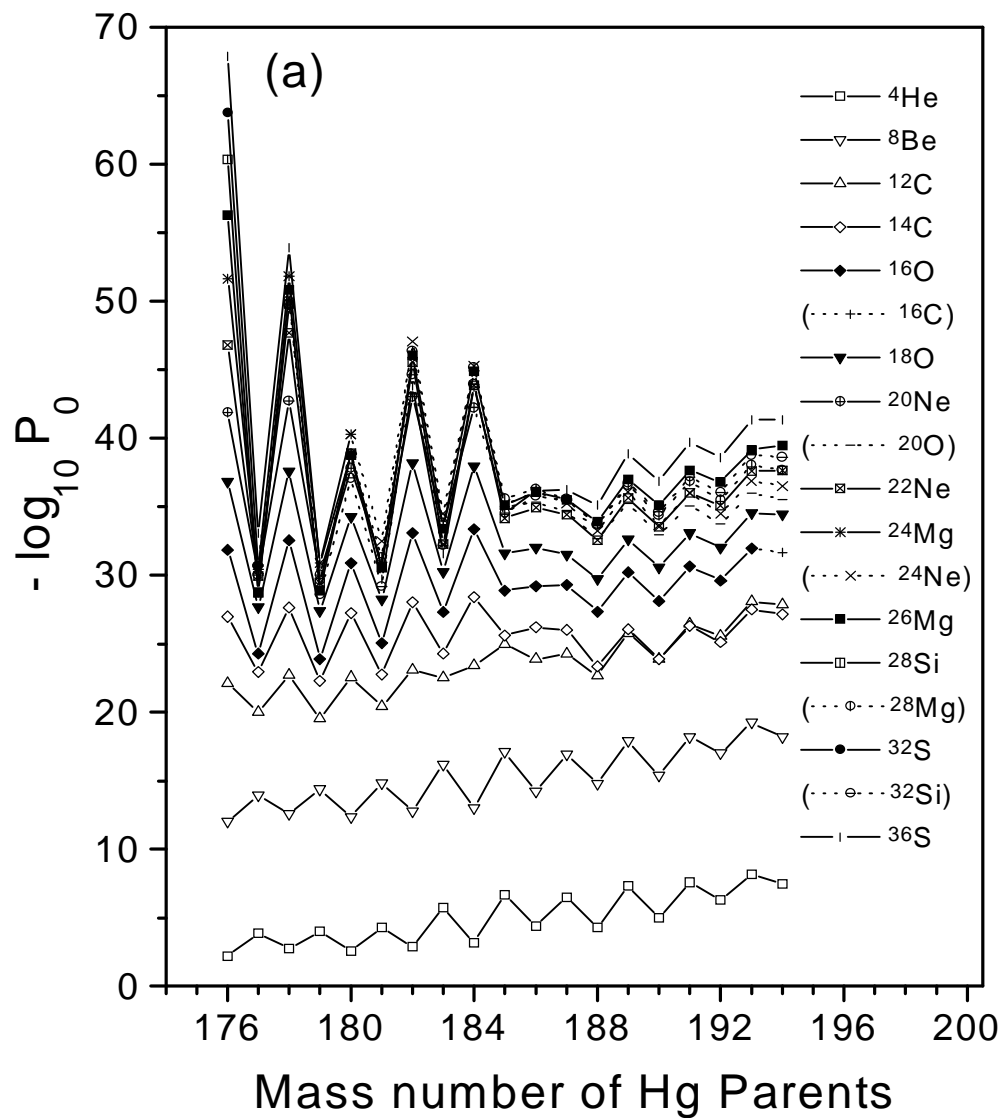


Fig. 6 "Closed shell effects from" R.K. Gupta et al.

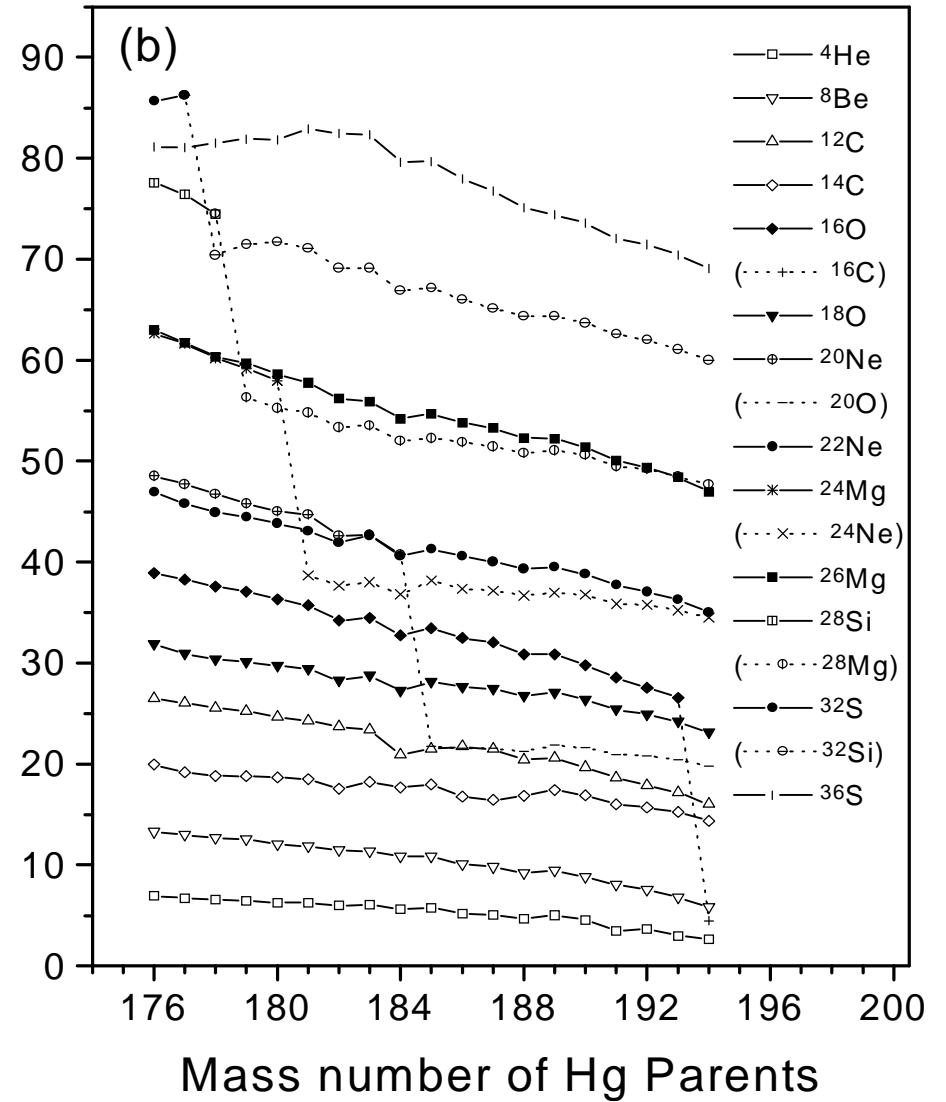
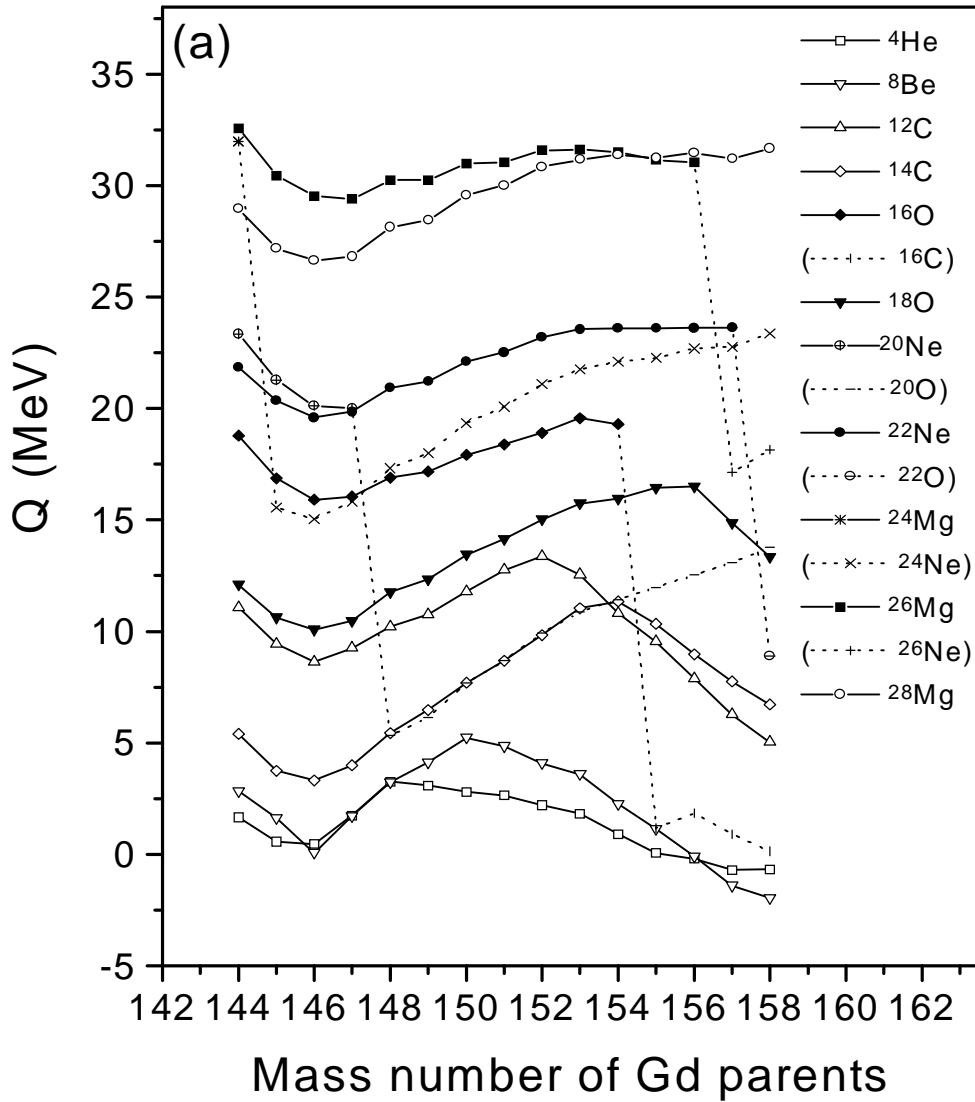


Fig. 7 "Closed shell effects from" R.K. Gupta et al.

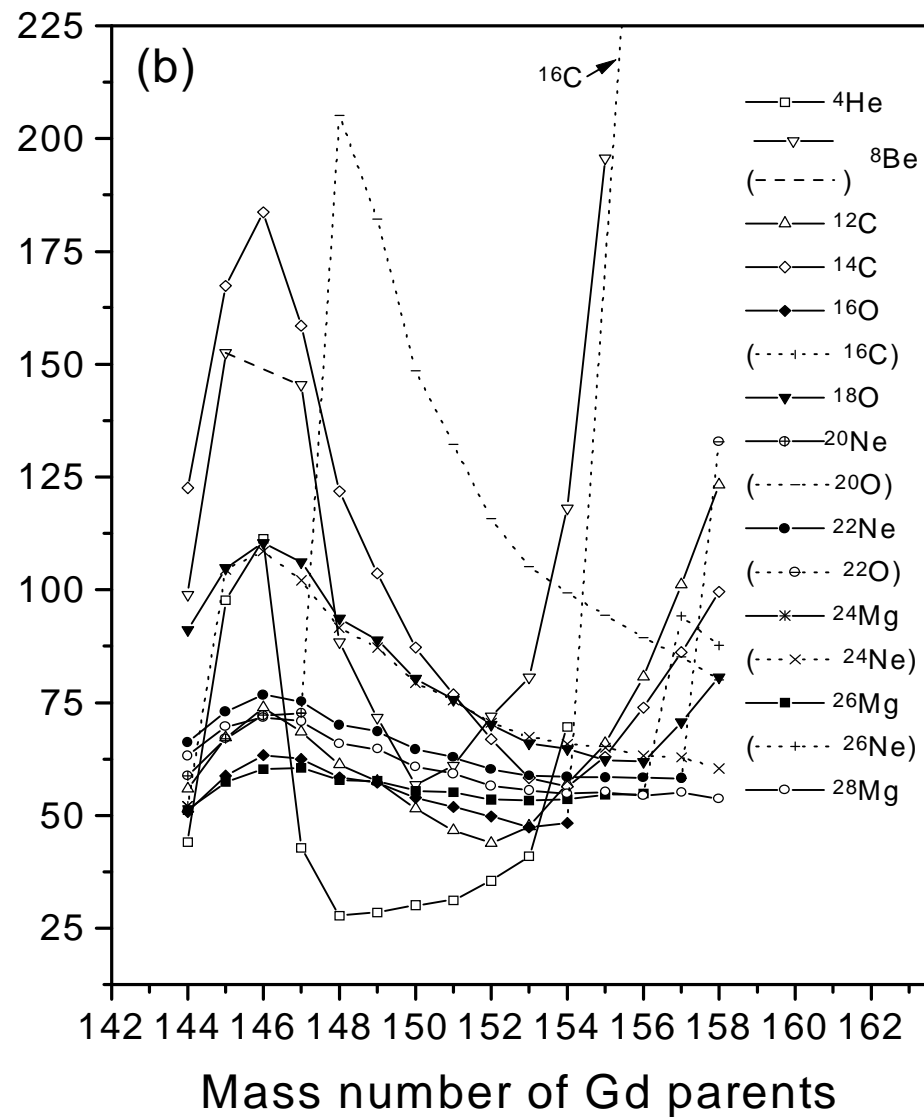
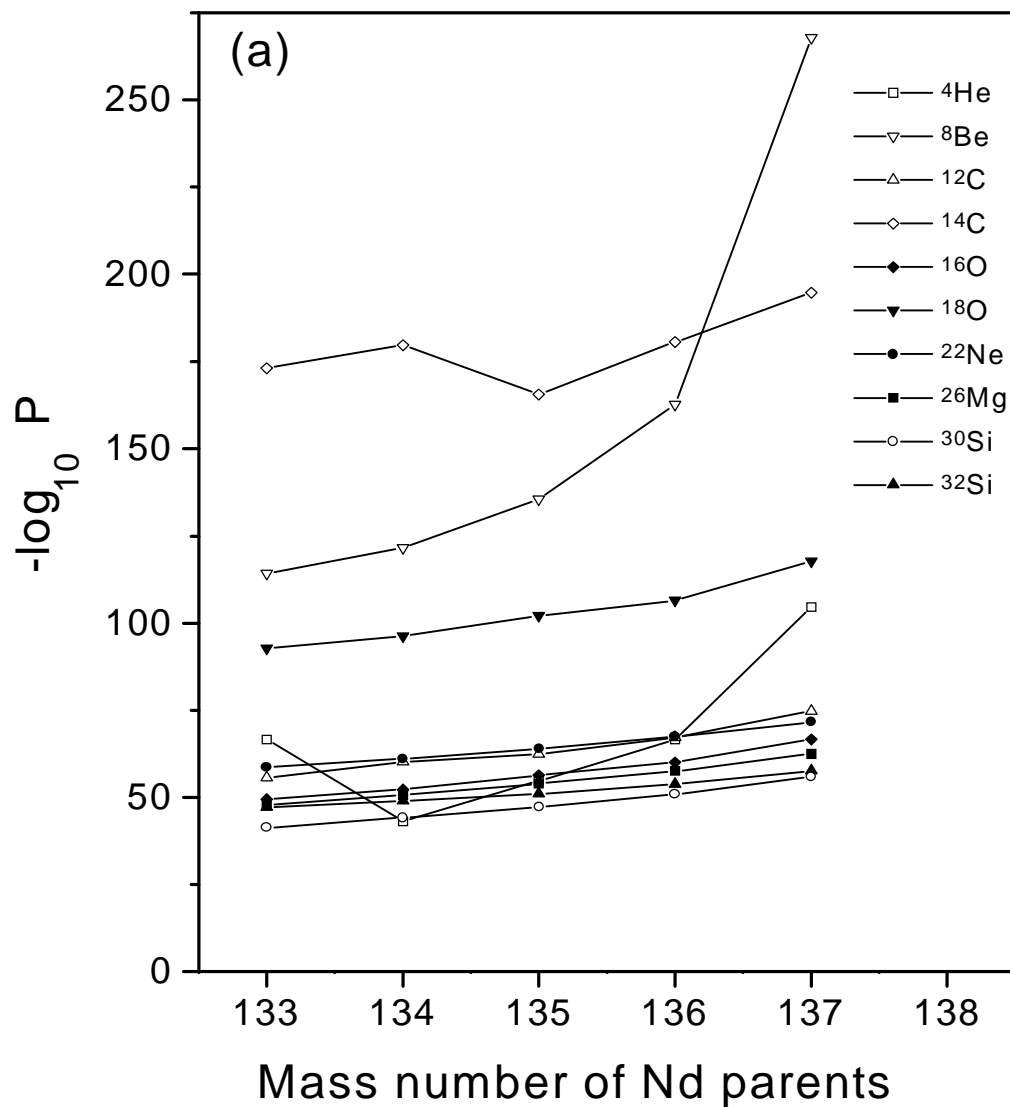


Fig. 8 "Closed shell effects from" R.K. Gupta et al.

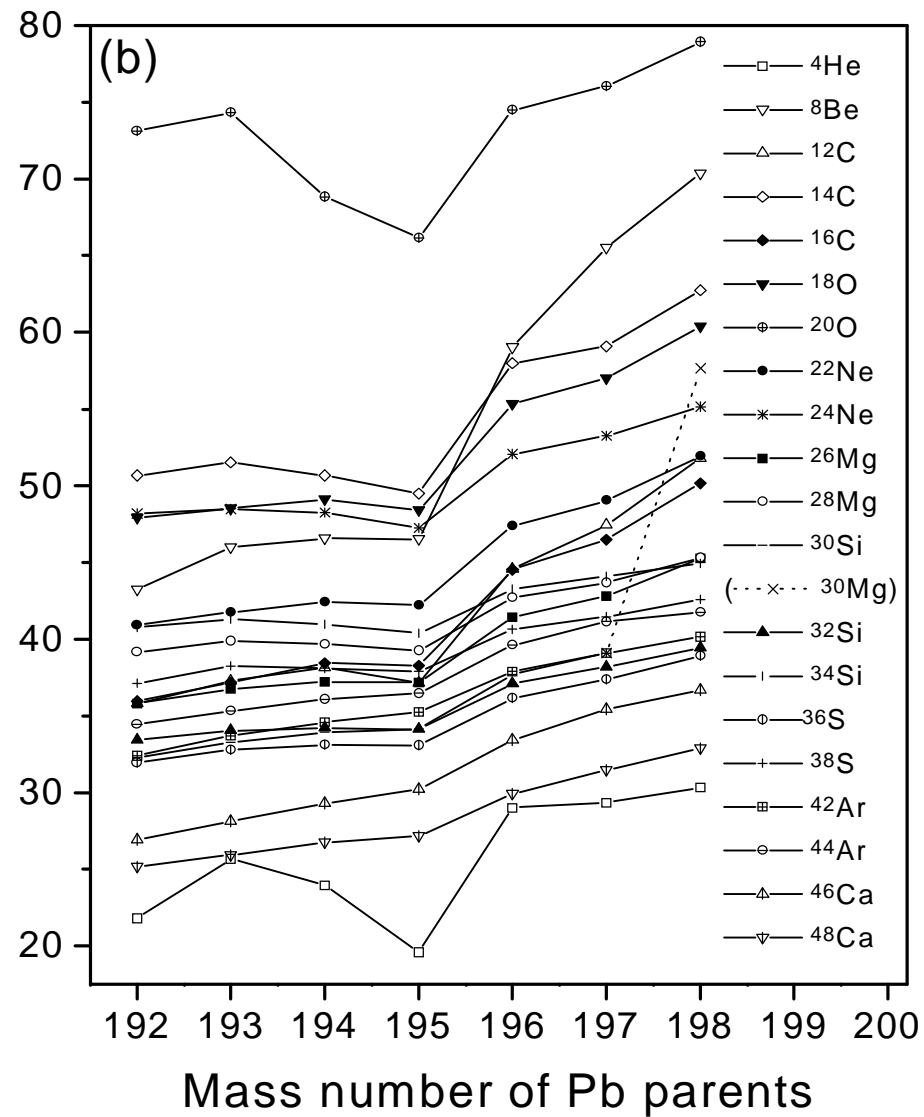
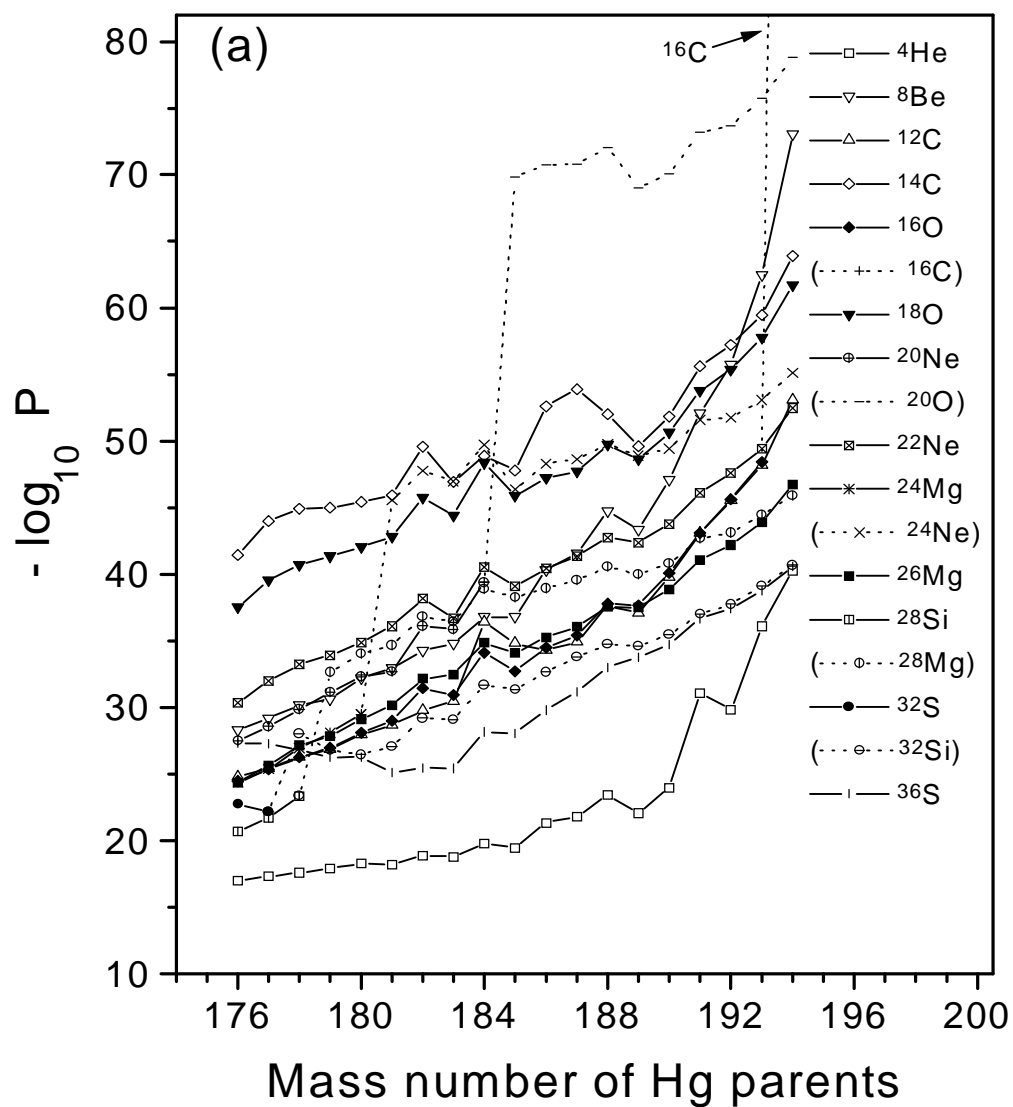


Fig. 9 "Closed shell effects from" R.K. Gupta et al.

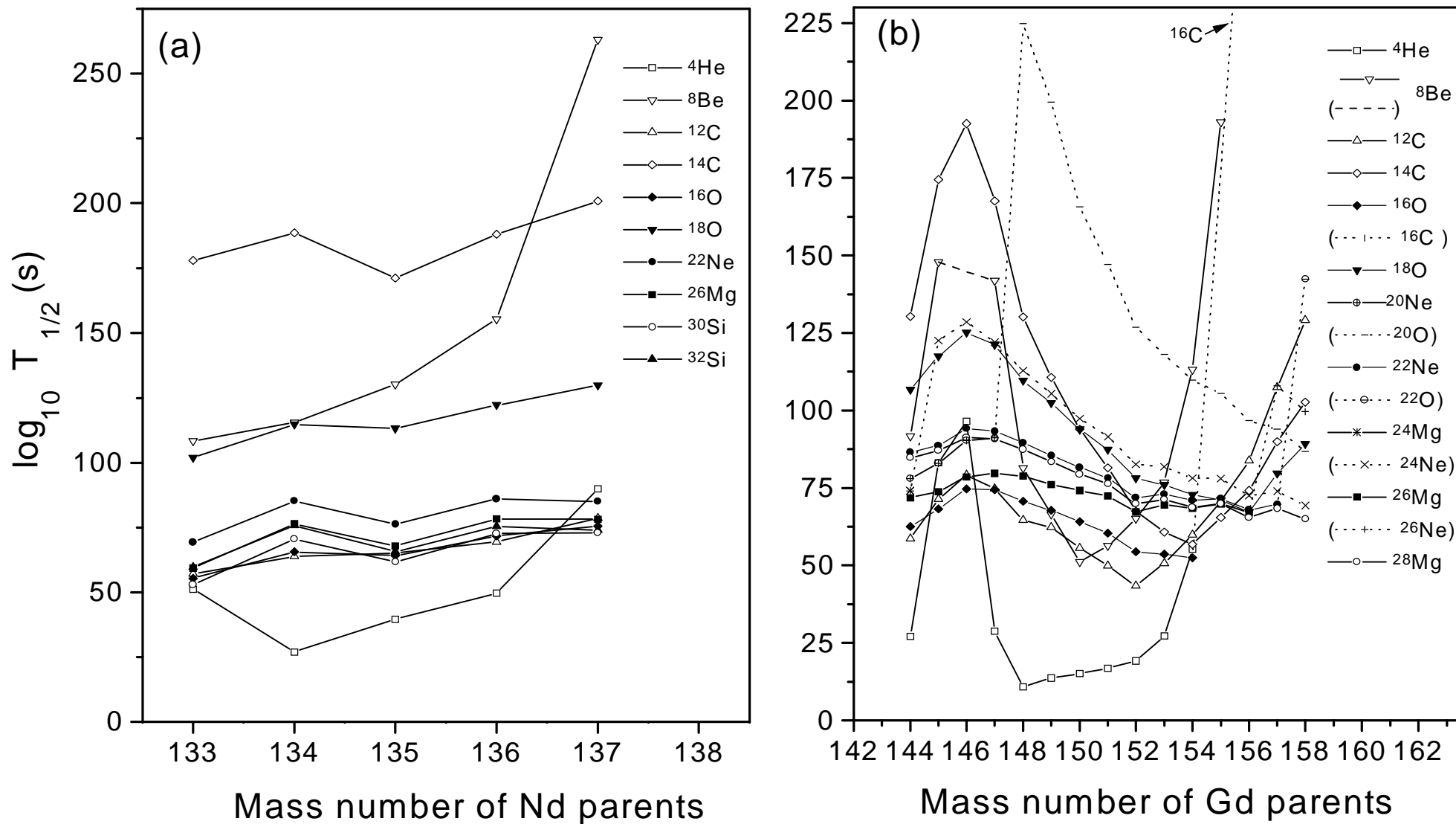


Fig. 10 "Closed shell effects from" R.K. Gupta et al.

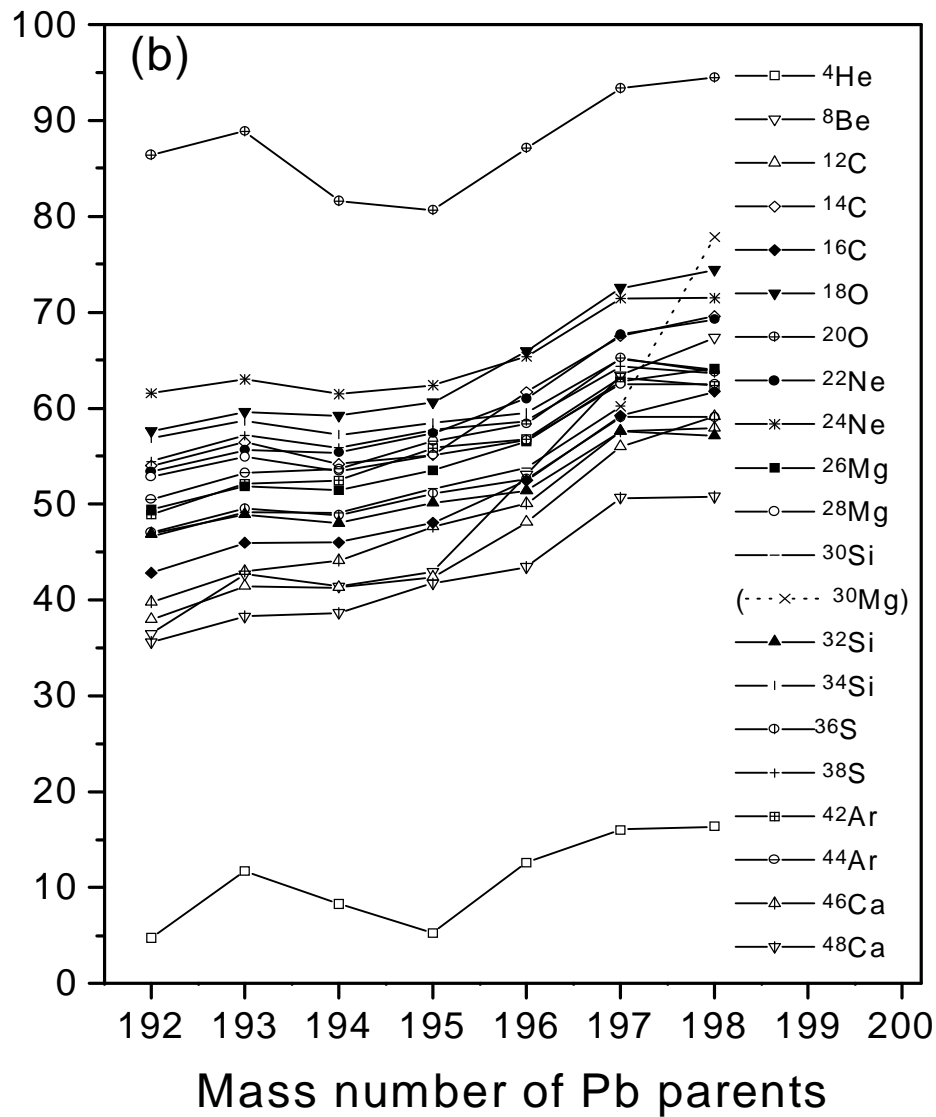
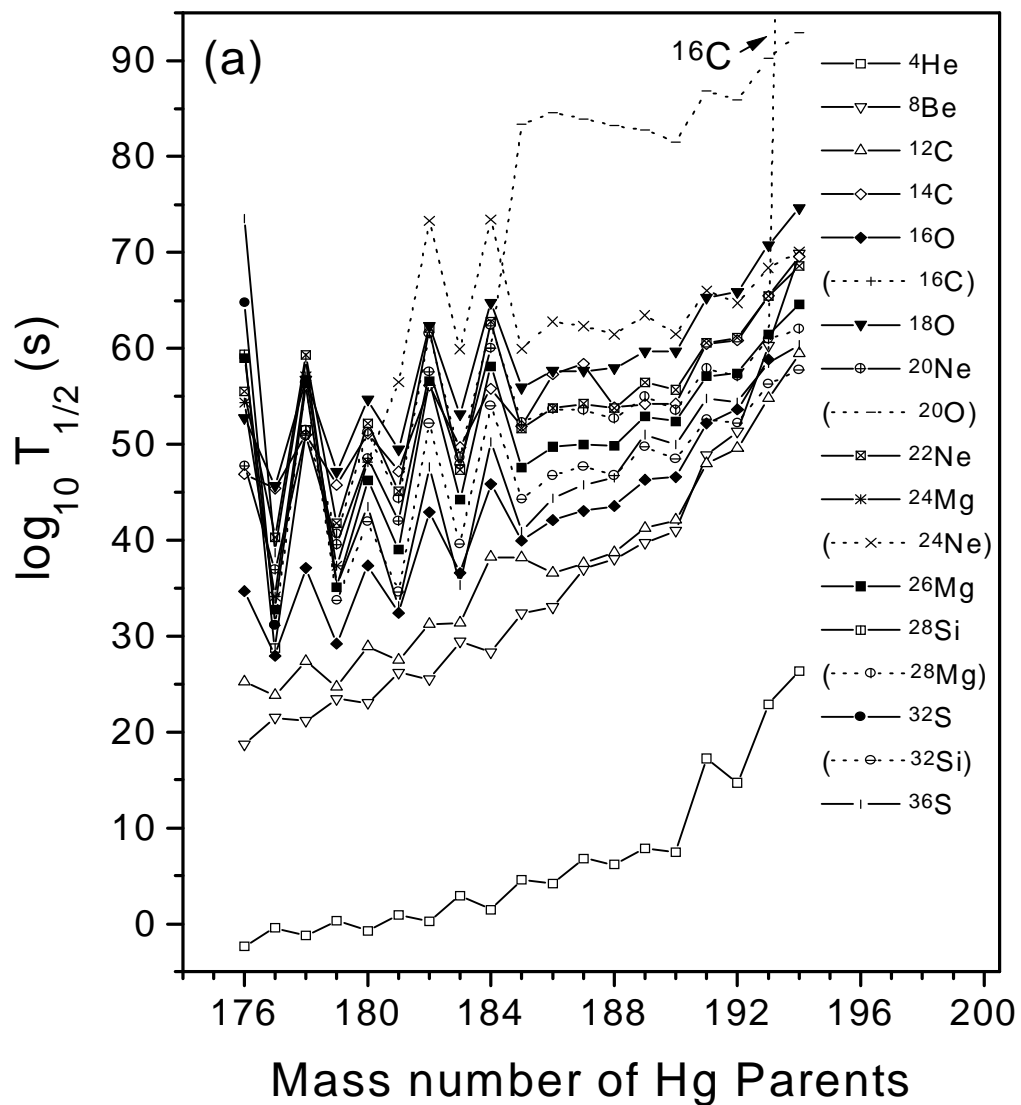


Fig. 11 "Closed shell effects from" R.K. Gupta et al.

